

Long-lived elementary excitations and light coherence in topological lasers

Petr Zapletal, Bogdan Galilo, and Andreas Nunnenkamp
Cavendish Laboratory, University of Cambridge, Cambridge CB3 0HE, United Kingdom
(Dated: February 28, 2020)

We study a topological laser based on the photonic Haldane model with selective pumping of chiral edge modes described by saturable gain. We investigate elementary excitations around the mean-field steady state and their consequences for the coherence properties. In particular, we show that the hybridization of chiral edge modes gives rise to long-lived elementary excitations, leading to large phase fluctuations in the emitted light field and a decrease of light coherence. The lifetime of elementary excitations strongly depends on the dispersion of edge-mode frequencies around the lasing frequency. As a result, the lifetime can be reduced by orders of magnitude for lasing of different edge modes, leading to the suppression of phase fluctuations and a large coherence of emitted light. On the other hand, amplitude fluctuations and the second-order autocorrelation function are moderately increased at the same time. We confirm our results by numerical simulations of semiclassical Langevin equations taking nonlinear noise dynamics into account.

I. INTRODUCTION

Topological photonics has made rapid strides in the past years [1], investigating effects of gain and loss on the topology of photonic energy bands [2], topology in synthetic dimensions [3] as well as the interplay of topology and nonlinear optics phenomena [4]. Lasing in topological photonic structures has recently attracted a lot of attention not only because it allows studying topology in a novel nonlinear non-Hermitian regime but also because topological structures can offer a new design of laser devices. First, lasing of zero-dimensional edge modes has been demonstrated in one-dimensional photonic arrays [5–7]. These pioneering works have been followed by experiments reporting lasing of one-dimensional chiral edge modes in two-dimensional photonic arrays [8–11]. In a two-dimensional array, lasing of a single edge mode extending over the whole edge of the photonic array has been demonstrated [9]. The single-mode laser operation is robust against on-site disorder in contrast to topologically trivial laser arrays [12]. For this reason, topological lasers are a promising candidate for highly-efficient lasers with a robust emission spectrum. The rich dynamics of topological lasers are subject to current theoretical investigation [13, 14]. However, the theory for coherence properties of topological lasers, which would be relevant for recent experiments demonstrating stable laser operation [9], has been still missing. Large spatial and temporal coherence of emitted light field is an essential characteristic of lasers, which is required for practical laser applications [15].

Here, we study elementary excitations and light coherence in a topological laser. We consider the Haldane model based on a two-dimensional photonic array pumped along the edge. On the mean-field level neglecting quantum and thermal fluctuations in the laser, we obtain lasing of a single edge mode. Depending on initial conditions, lasing of edge modes with different lasing frequencies can be achieved as it was described in Ref. [14]. We take fluctuations into account using nonlinear semiclassical Langevin equations. We linearize the

Langevin equations around the mean-field steady-state solution to study elementary excitations. We consider weak gain and loss in comparison to the coupling of optical sites in the array and a moderate size of the array such that the frequency separation of edge modes is larger than the linewidth of these modes. This regime is relevant for recent experiments [9, 16]. We study how normal modes of elementary excitations are formed from the normal modes of a passive system, which does not experience either gain or loss. We show that the hybridization of edge modes gives rise to long-lived elementary excitations, which lead to large phase fluctuations and a decreased coherence of the emitted light field. Since topological edge modes and their frequencies are robust against disorder, the long-lived elementary excitations appear even if moderate on-site disorder is considered. The lifetime of elementary excitations strongly depends on the dispersion of edge-mode frequencies around the lasing frequency. Any deviation from a linear dispersion leads to a detuning for normal modes of elementary excitations, which can obstruct their hybridization and, as a consequence, reduce their lifetime. For lasing at frequencies, which do not lie in the middle of the passive-system band gap, the deviation from a linear dispersion is sufficient to reduce the lifetime of elementary excitations by at least one order of magnitude. This leads to a large suppression of phase fluctuations and an increase of light coherence. On the other hand, amplitude fluctuations of the emitted light field are increased resulting in a moderately larger second-order autocorrelation function. We confirm our results by numerical simulations of full Langevin equations, which take nonlinear noise dynamics into account.

II. MODEL

We consider an array of optical sites, whose complex amplitudes c_j , $j = 1, \dots, N$, are described by the semi-

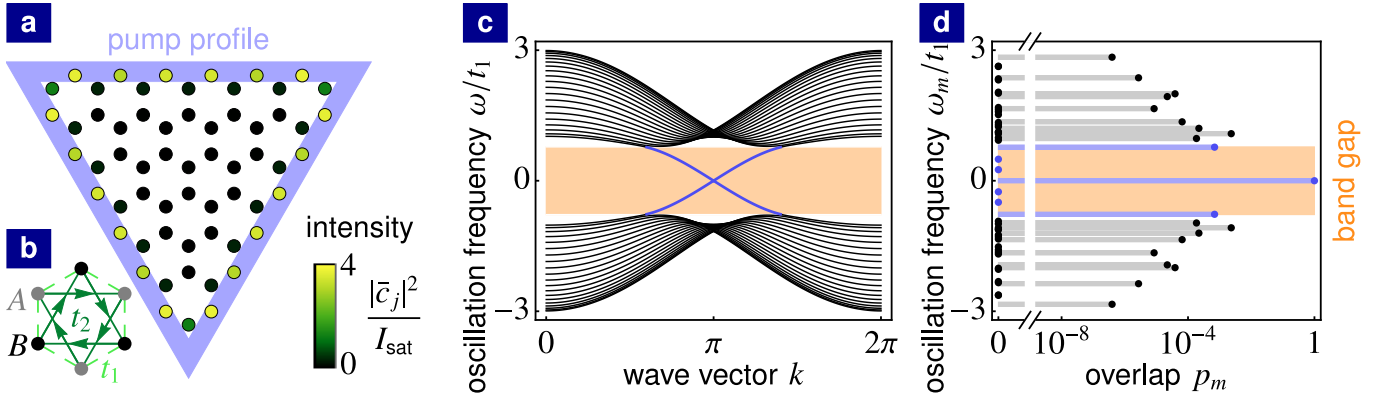


FIG. 1. Mean-field steady state of topological laser. (a) The honeycomb photonic array with photon tunneling described by the Haldane model pumped in the blue region. The color scale shows the mean-field steady state occupations $|\bar{c}_j|^2$ of local optical sites. (b) Unit cell of the Haldane model consisting of the sublattice A (gray points), the sublattice B (black points), the nearest-neighbor hopping with a real tunneling t_1 and the next-nearest-neighbor hopping with a complex amplitude $t_2 e^{i\phi_{jk}}$. (c) Band structure of the passive Haldane model (no gain no loss) with bulk modes (black lines), topological band gap (orange region) and topological edge modes (blue lines) for an infinite strip with zig-zag edges. (d) The overlap p_m of the mean-field steady-state solution with normal modes $e^{(m)}$ of the passive system (no gain no loss) for the mode with frequency $\Omega/t_1 = 0$ lasing. (Parameters: $t_2/t_1 = 0.15$, $\phi = \pi/2$, $\gamma/t_1 = 0.01$, $g/t_1 = 0.05$, $N = 61$)

classical Langevin equations

$$i \frac{d}{dt} c_j = \left[\omega_j - i\gamma + i \frac{\mathbb{P}_j g}{1 + \frac{|\bar{c}_j|^2}{I_{\text{sat}}}} \right] c_j + \sum_{k=1}^N H_{jk} c_k + Q_{jk} c_{j,\text{in}}, \quad (1)$$

where $\hbar = 1$, ω_j are the frequencies of the optical sites, the Hamiltonian H_{jk} describes the coupling of these sites, and N is the number of the optical sites in the array. Intrinsic optical losses lead to a decay at rate γ . Incoherent pumping of optical sites is described by a saturable gain g , where I_{sat} is the saturation intensity. We allow for a spatial pump profile where $\mathbb{P}_j = 1$ for pumped sites and $\mathbb{P}_j = 0$ for not pumped sites. Optical losses and incoherent pumping lead to shot noise and thermal noise, respectively, which are described by Gaussian white noise $\langle c_{j,\text{in}}(t) c_{k,\text{in}}^*(t') \rangle = \delta_{jk} \delta(t - t')$ with a correlation matrix $\mathbf{Q} \mathbf{Q}^\dagger$, where \mathbf{Q} is a diagonal matrix, $Q_{jk} = \delta_{jk} [\sqrt{2\gamma(1 - \mathbb{P}_j)} + \sqrt{q} \mathbb{P}_j]$, and δ_{jk} is the Kronecker delta. To account for thermal noise in addition to shot noise at pumped optical sites, we consider a larger variance $q \geq 2\gamma$ of the Gaussian white noise at the pumped sites.

We focus on the Haldane Hamiltonian $\hat{H} = t_1 \sum_{\text{n.n.}} \hat{c}_j^\dagger \hat{c}_k + t_2 \sum_{\text{n.n.n.}} e^{i\phi_{jk}} \hat{c}_j^\dagger \hat{c}_k$ based on a honeycomb array (see Fig 1b) including the nearest-neighbor hopping with a real amplitude t_1 and the next-nearest-neighbor hopping with a complex amplitude $t_2 e^{i\phi_{jk}}$ [17, 18]. $\phi_{jk} = \phi$ for hopping in the directions shown by green arrows in Fig 1b and $\phi_{jk} = -\phi$ in the reverse directions, where ϕ is the Haldane flux. In Fig. 1c, we plot the band structure of the passive Haldane model (black lines) for no gain and no loss in the photonic array. For $\phi \neq 0, \pi$, the time-reversal symmetry of the system is broken and a topological band gap opens (orange region). Cutting

the array in a form of an infinite strip, chiral edge modes (blue lines) appear at the boundaries of the array. Frequencies of the chiral edge modes lie in the topological band gap.

III. MEAN-FIELD STEADY STATE

We first find steady states of the mean-field dynamical equations for optical amplitudes, which are obtained by omitting stochastic terms in the Langevin equations (1). We consider a finite array depicted in Fig. 1a, where optical sites in the blue region are pumped. We assume that gain and loss are weak in comparison to the hopping amplitudes, i.e. $g, \gamma \ll t_1, t_2$. In this regime, lasing of a single topological edge mode is achieved [9]. In Fig. 1d, we show the overlap $p_m = |\sum_{j=1}^N \bar{c}_j^* e_j^{(m)}| / \sqrt{\sum_{j=1}^N |\bar{c}_j|^2}$ of the mean-field steady state solution \bar{c}_j with the normal modes $e^{(m)}$ of the passive system (no gain no loss). Depending on the initial conditions, one of the edge modes wins the gain competition. Since all edge modes extend across the whole pump region, a single edge mode saturates gain at all pumped optical sites and prevents lasing of other edge modes. As a result, the overlap of the mean-field steady state with a single edge mode is close to unity and the overlaps with the remaining passive-system normal modes is very small. Lasing of different edge modes leads to different lasing frequencies and different steady-state distributions of optical phases $\bar{\theta}_j$ along the edge of the array (see Fig. 2a and 2b). However, the occupation of optical sites, $|\bar{c}_j|^2$, (see Fig. 1a) is almost identical for lasing of any edge mode, since all edge modes have very similar spatial profile $|e_j^{(m)}|^2$. The mean-field dynamics of complex amplitudes $c_j / \sqrt{I_{\text{sat}}}$ and the mean-field steady

state $\bar{c}_j/\sqrt{I_{\text{sat}}}$ are independent of the absolute scaling I_{sat} .

IV. ELEMENTARY EXCITATIONS

In this section, we describe elementary excitations around the mean-field steady state. We show how the normal modes of elementary excitations are formed from the passive-system normal modes.

To study elementary excitations around the mean-field steady state, we decompose optical amplitudes $c_j = (\bar{c}_j + \delta c_j) e^{-i\Omega t}$ into the mean-field steady-state solution \bar{c}_j and a modulation δc_j , where Ω is the frequency of the lasing mode. Considering small modulations around the mean-field steady state, we derive linear Langevin equations

$$i \frac{d}{dt} \begin{pmatrix} \delta \mathbf{c} \\ \delta \mathbf{c}^* \end{pmatrix} = \mathcal{D} \begin{pmatrix} \delta \mathbf{c} \\ \delta \mathbf{c}^* \end{pmatrix} + \mathcal{Q} \begin{pmatrix} \mathbf{c}_{\text{in}} e^{i\Omega t} \\ \mathbf{c}_{\text{in}}^* e^{-i\Omega t} \end{pmatrix}, \quad (2)$$

where \mathcal{D} is the dynamical matrix for elementary excitations around the mean-field steady state, $\mathcal{Q} = \mathbf{Q} \otimes \sigma_z$ and σ_z is the Pauli matrix. The dynamical matrix

$$\mathcal{D} = \mathcal{H} + \mathcal{A} = \begin{pmatrix} \mathbf{H} - \Omega \mathbb{1} & 0 \\ 0 & -\mathbf{H}^* + \Omega \mathbb{1} \end{pmatrix} + i \begin{pmatrix} \mathbf{\Gamma} & \mathbf{\Delta} \\ \mathbf{\Delta}^* & \mathbf{\Gamma} \end{pmatrix} \quad (3)$$

can be decomposed into the Hermitian part \mathcal{H} and the anti-Hermitian part \mathcal{A} , where H_{jk} is the Hamiltonian of the passive system, $\mathbb{1}$ is the $N \times N$ identity matrix,

$$\Gamma_{jj} = -\gamma + \frac{\mathbb{P}_j g}{\left(1 + \frac{|\bar{c}_j|^2}{I_{\text{sat}}}\right)^2}, \quad \Delta_{jj} = -\frac{\mathbb{P}_j g \frac{\bar{c}_j^2}{I_{\text{sat}}}}{\left(1 + \frac{|\bar{c}_j|^2}{I_{\text{sat}}}\right)^2}, \quad (4)$$

and $\Gamma_{jk} = \Delta_{jk} = 0$ for $j \neq k$. The dynamical matrix depends only on rescaled mean-field optical amplitudes $\bar{c}_j/\sqrt{I_{\text{sat}}}$. As a result, elementary excitations do not depend on the absolute scaling, I_{sat} , of the mean-field optical amplitudes.

For elementary excitations, the number of normal modes is doubled compared to the number of the passive-system normal modes. The dynamical matrix \mathcal{D} exhibits the following symmetry $\mathcal{X} \mathcal{D} \mathcal{X} = -\mathcal{D}^*$ where $\mathcal{X} = \mathbb{1} \otimes \sigma_x$ and σ_x is the Pauli matrix. Due to this symmetry, the complex frequencies $\epsilon^{(\alpha)}$, $\alpha = 1, \dots, 2N$, of elementary excitations are purely imaginary or appear in pairs $(\epsilon^{(\alpha)}, \tilde{\epsilon}^{(\alpha)})$, where $\tilde{\epsilon}^{(\alpha)} = -(\epsilon^{(\alpha)})^*$.

We first diagonalize the Hermitian part \mathcal{H} by switching to the basis of passive-system normal modes $\mathcal{E}_p^{(m)} = \mathbf{e}^{(m)} \otimes (1, 0)^T$ and $\tilde{\mathcal{E}}_p^{(m)} = (\mathbf{e}^{(m)})^* \otimes (0, 1)^T$, where $\mathbf{e}^{(m)}$, $m = 1, \dots, N$, are eigenmodes of \mathbf{H} . The eigenfrequencies of the Hermitian part are directly formed from the passive-system eigenfrequencies ω_m , giving rise to two branches $\epsilon_p^{(m)} = \omega_m - \Omega$ and $\tilde{\epsilon}_p^{(m)} = -\omega_m + \Omega$. The anti-Hermitian part

$$\tilde{\mathcal{A}} = i \begin{pmatrix} \tilde{\mathbf{\Gamma}} & \tilde{\mathbf{\Delta}} \\ \tilde{\mathbf{\Delta}}^* & \tilde{\mathbf{\Gamma}}^* \end{pmatrix} \quad (5)$$

introduces coupling between passive-system normal modes, where $\tilde{\mathbf{\Gamma}} = \mathbf{U}^\dagger \mathbf{\Gamma} \mathbf{U}$, $\tilde{\mathbf{\Delta}} = \mathbf{U}^\dagger \mathbf{\Delta} \mathbf{U}^*$. Columns of the transformation matrix \mathbf{U} are eigenmodes $\mathbf{e}^{(m)}$. Due to the anti-Hermitian coupling, the passive-system normal modes hybridize.

We now discuss the coupling of modes, $\mathcal{E}_p^{(m)}$ and $\tilde{\mathcal{E}}_p^{(n)}$, from the two different branches due to the off-diagonal sectors $\tilde{\mathbf{\Delta}}$ and $\tilde{\mathbf{\Delta}}^*$ of the dynamical matrix. The coupling between modes $\mathcal{E}_p^{(m)}$ and $\tilde{\mathcal{E}}_p^{(n)}$ is described by the 2×2 dynamical matrix

$$\tilde{\mathcal{D}}^{(m,n)} = \begin{pmatrix} \omega_m - \Omega & 0 \\ 0 & -\omega_n + \Omega \end{pmatrix} + i \begin{pmatrix} \tilde{\Gamma}_{mm} & \tilde{\Delta}_{mn} \\ \tilde{\Delta}_{nm}^* & \tilde{\Gamma}_{nn} \end{pmatrix}, \quad (6)$$

if their frequencies are isolated from the rest of the passive-system spectrum, i.e. $|\omega_{m/n} + \omega_q - 2\Omega| \gg |\tilde{\Delta}_{m/nq}|$, $|\omega_{m/n} - \omega_q| \gg \tilde{\Gamma}_{m/nq}$ for all $q \neq m, n$. Diagonalizing the 2×2 dynamical matrix, we obtain complex frequencies of hybridized modes

$$\epsilon_{\pm}^{(m,n)} = \bar{\omega}_{mn} - i\tilde{\Gamma}_{mn} \pm \frac{1}{2} \sqrt{(\delta\omega_{mn} + i\delta\Gamma_{mn})^2 - 4|\tilde{\Delta}_{mn}|^2}, \quad (7)$$

where $\bar{\omega}_{mn} = (\omega_m - \omega_n)/2$, $\delta\omega_{mn} = \omega_m + \omega_n - 2\Omega$, $\tilde{\Gamma}_{mn} = -(\tilde{\Gamma}_{mm} + \tilde{\Gamma}_{nn})/2$, and $\delta\Gamma_{mn} = \tilde{\Gamma}_{mm} - \tilde{\Gamma}_{nn}$. The real parts of complex frequencies correspond to oscillation frequencies and the imaginary parts of complex frequencies correspond to decay rates or amplification rates. The real part and the imaginary part of the complex frequencies $\epsilon_{\pm}^{(m,n)}$ are shown in Figs. 2e and 2f, respectively, as a function of the detuning $\delta\omega_{mn}$. One can see that due to the anti-Hermitian coupling of passive-system normal modes, the real parts of the complex frequencies are attracted to each other, $\text{Re}(\epsilon_+^{(m,n)} - \epsilon_-^{(m,n)}) < |\delta\omega_{mn}|$. On the other hand, the imaginary parts of the complex frequencies split. This is an example of level attraction, which is a general concept appearing in various physical platforms [19–21]. For $2\tilde{\Gamma}_{mn} > \sqrt{\delta\Gamma_{mn} + 4|\tilde{\Delta}|^2}$, both hybridized modes decay as the imaginary parts of the complex frequencies are negative. The splitting in the imaginary parts of the complex frequencies is large for small detunings $\delta\omega$ leading to a slowly-decaying mode and a fast-decaying mode. For a large detuning $|\delta\omega_{mn}| \gg |\tilde{\Delta}_{mn}|$, the hybridization is negligible and the frequencies of uncoupled modes $\epsilon_+^{(m,n)} \approx \omega_m - \Omega + i\tilde{\Gamma}_{mm}$ as well as $\epsilon_-^{(m,n)} \approx -\omega_n + \Omega + i\tilde{\Gamma}_{nn}$ are recovered.

The hybridization of passive-system normal modes from the two different branches described by the 2×2 dynamical matrix $\tilde{\mathcal{D}}^{(m,n)}$ will be shown in the next section to have important consequences for the complex spectrum of elementary excitations.

V. SPECTRUM OF ELEMENTARY EXCITATIONS

We now investigate the complex spectrum of elementary excitations in the regime $t_1, t_2 \gg g, \gamma$. In Fig. 2d, we

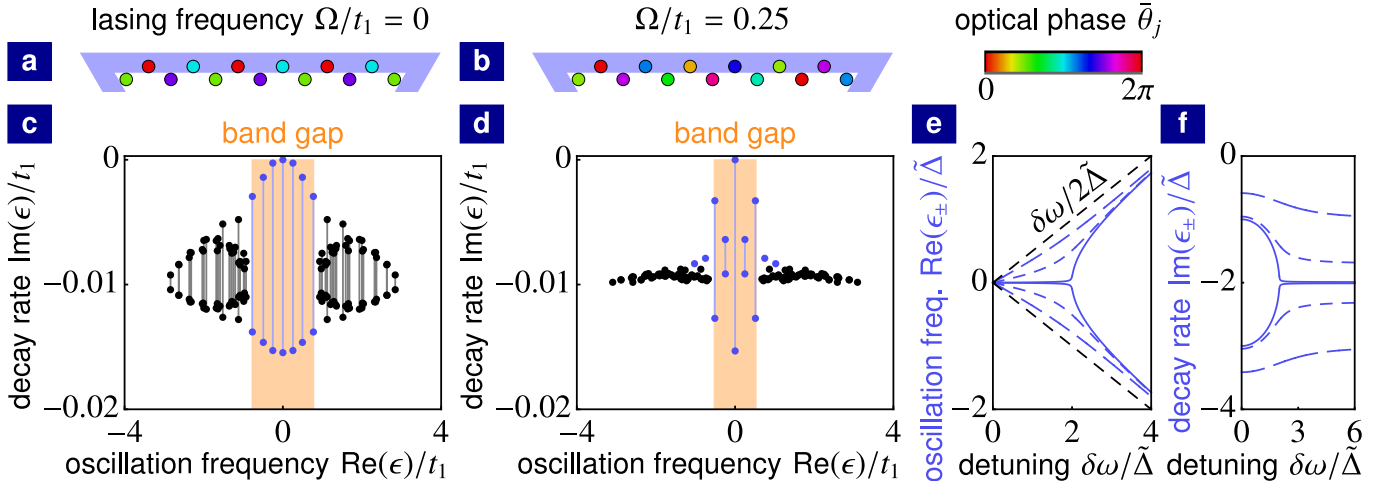


FIG. 2. Elementary excitations for lasing of different edge modes. (a) and (b) Mean-field steady-state distribution of optical phases along the top edge of the photonic array for the lasing frequency $\Omega/t_1 = 0$ and $\Omega/t_1 = 0.25$, respectively. (c) and (d) Complex spectrum of elementary excitations with band gap (orange region), bulk modes (black points) as well as edge modes (blue points) for the lasing frequency $\Omega/t_1 = 0$ and $\Omega/t_1 = 0.25$, respectively. Grey and blue lines show the splitting in imaginary parts of complex frequencies due to the hybridization of bulk modes and edge modes, respectively. (e) and (f) Real part and imaginary part, respectively, of complex frequencies ϵ_{\pm} for two hybridized modes as a function of the detuning $\delta\omega$ for different values of the decay-rate difference $\delta\Gamma/\tilde{\Delta} = 0.02$ (full lines), $\delta\Gamma/\tilde{\Delta} = 0.6$ (dashed lines) and $\delta\Gamma/\tilde{\Delta} = 2$ (dot-dashed lines). (Parameters: (a-d) $t_2/t_1 = 0.15$, $\phi = \pi/2$, $\gamma//t_1 = 0.01$, $g/t_1 = 0.05$, $N = 61$; (e) and (f) $\bar{\omega}/\tilde{\Delta} = 0$, $\bar{\Gamma}/\tilde{\Delta} = -2$)

plot the complex spectrum of elementary excitations for lasing of the edge mode with the frequency $\Omega/t_1 = 0.25$. This spectrum reveals generic features of elementary excitations in topological lasers.

Normal modes of elementary excitations are formed from either bulk modes (black points) or edge modes (blue points) of the passive system. In the regime $t_1, t_2 \gg g, \gamma$, the oscillation frequencies (real parts of complex frequencies) of elementary excitations are predominantly determined by the eigenfrequencies of the Hermitian part \mathcal{H} , which consists of two branches $\epsilon_p^{(m)} = \omega_m - \Omega$ and $\tilde{\epsilon}_p^{(m)} = -\omega_m + \Omega$ formed from the passive system frequencies ω_m . These two branches are shifted in respect to each other by the lasing frequency Ω . Since the lasing frequency $\Omega/t_1 = 0.25$ does not lie in the middle of the passive-system band gap, the band gap in the spectrum of elementary excitations (orange region in Fig. 2d) is smaller than the passive-system band gap. Frequencies of some edge modes lie within the bulk bands.

All imaginary parts of complex frequencies are negative (except from a single frequency with a vanishing imaginary part discussed later) confirming the stability of the steady state. Here $|\omega_m - \omega_n| \gg g, \gamma$ for all $m \neq n$ and edge-mode frequencies ω_m lying in the band gap of the passive system. As a result, every edge mode $\epsilon_p^{(m)}$ can significantly hybridize only with a single mode $\tilde{\epsilon}_p^{(n)}$ from the other branch and their coupling is described by the 2×2 dynamical matrix (6). Due to the large spatial overlap of edge modes in the pumped region \mathbb{P}_j , the coupling $|\tilde{\Delta}_{mn}|$ between edge modes overcomes the detuning of their passive-system frequencies $|\delta\omega_{mn}|$. This

leads to a large hybridization of edge modes and to a distinctive splitting in the imaginary parts of their complex frequencies (blue lines in Fig. 2d).

Two passive-system normal modes formed from the lasing mode $\mathbf{e}^{(l)}$ are always degenerate at frequency $\epsilon_p^{(l)} = \tilde{\epsilon}_p^{(l)} = 0$. The hybridization of these two modes gives rise to a non-decaying mode with the complex frequency $\epsilon_{+}^{(l,l)} = 0$ and a fast-decaying mode with the complex frequency $\epsilon_{-}^{(l,l)} = -2i\bar{\Gamma}u$ (see Appendix A for more details). These non-decaying and fast-decaying excitations correspond to undamped fluctuations in the phase of the lasing mode and largely-damped fluctuations in the amplitude of the lasing mode, respectively, which are characteristic for a laser driven above threshold [22].

Note that the hybridization of edge modes $\epsilon_p^{(m)}$ and $\tilde{\epsilon}_p^{(n)}$ from the same branch is negligible because the detuning of passive-system frequencies $|\delta\omega_{mn}| = |\omega_m - \omega_n|$ is always larger than the coupling term $|\tilde{\Gamma}_{mn}|$ between these modes.

Since couplings $\tilde{\Delta}_{nm}$ and $\tilde{\Gamma}_{nm}$ between bulk modes are small, the hybridization of bulk modes is typically also negligible. Complex frequencies of non-hybridized bulk modes (black points in Fig. 2d) acquire imaginary parts $\text{Im} \epsilon^{(m)} \approx -\gamma$ and $\text{Im} \tilde{\epsilon}^{(m)} \approx -\gamma$ due to the diagonal term $\tilde{\Gamma}_{mm} \approx -\gamma$ in the anti-Hermitian part of the dynamical matrix.

Note that for the value of the Haldane flux $\phi = \pi/2$, a small hybridization of bulk modes occurs for lasing at the frequency $\Omega/t_1 = 0$ (see Fig. 2c), because bulk modes are pairwise degenerate due to the symmetry, $\mathbf{S} \mathbf{H} \mathbf{S} = -\mathbf{H}^*$, of the passive-system Hamiltonian \mathbf{H} , where \mathbf{S} is a uni-

tary and $\mathbf{S}^2 = \mathbb{1}$ (see Appendix B for more details). However, the splitting in imaginary parts of complex frequencies for bulk modes is small in comparison to the splitting for edge modes and the hybridization of bulk modes does not appear for other values of the Haldane flux $\phi \neq \pi/2$ or for other lasing frequencies $\Omega/t_1 \neq 0$.

VI. LONG-LIVED ELEMENTARY EXCITATIONS

We now discuss long-lived elementary excitations, which occur in the Haldane model for lasing at a frequency lying in the middle of the passive-system band gap (vicinity of $\Omega/t_1 = 0$ for $\phi \approx \pi/2$).

In Fig. 2c, we plot the complex spectrum of elementary excitations for lasing at the frequency $\Omega/t_1 = 0$, which lies in the middle of the passive-system band gap. Long-lived elementary excitations with decay rates, which are orders of magnitude smaller than any other energy scale in the system (γ, g, t_1 and t_2), appear due to a large hybridization of edge modes. This is in contrast to lasing at the frequency $\Omega/t_1 = 0.25$ (see Fig. 2d), for which the decay rates of slowly-decaying modes are comparable to γ .

To understand the dependence of the spectrum for elementary excitations on the selection of a lasing edge mode, we can expand the edge-mode frequencies $\omega_m = \Omega + v_1(m-l) + v_2(m-l)^2 + \mathcal{O}((m-l)^3)$ around the lasing frequency Ω , where the index l labels the lasing mode. For $|v_1| \gg |v_2|$, the frequency of edge mode m is close to the frequency of edge mode $2l-m$ from the other branch of passive-system normal modes and their detuning is $\delta\omega_{m(2l-m)} = 2v_2(m-l)^2 + \mathcal{O}((m-l)^4)$. If the nonlinear coefficient $|v_2|$ and, as a consequence, also the detuning $\delta\omega_{m(2l-m)}$ are small compared to the coupling $|\tilde{\Delta}_{m(2l-m)}|$ between the edge modes, the edge modes significantly hybridize giving rise to a large splitting in the imaginary part of the complex frequencies, see Eq. (7) and Fig. 2f. On the other hand, if the nonlinear coefficient $|v_2|$ is comparable to or larger than the coupling $|\tilde{\Delta}_{m(2l-m)}|$, the resulting detuning $\delta\omega_{m(2l-m)}$ obstructs the hybridization and the splitting in the imaginary parts of edge-mode frequencies is reduced.

For the Haldane model, the dispersion of edge-mode frequencies is linear in the middle of the passive-system band gap for any $\phi \neq 0, \pi$. As v_2 is very small for lasing at a frequency lying in the middle of the passive-system band gap, long-lived elementary excitations, whose decay rate is orders of magnitude smaller than any other energy scale in the system (γ, g, t_1 and t_2), appear for any value of the Haldane flux. This can be seen in Fig. 3c, where we plot the smallest decay rate $\min_{\alpha \neq \nu} |\text{Im } \epsilon^{(\alpha)}|$ (index ν labels the non-decaying mode) as a function of the lasing frequency Ω for different values of the Haldane flux. On the other hand, for lasing at any frequency, which does not lie in the middle of the passive-system band gap, the

nonlinear coefficient v_2 is large enough to give rise to a considerable detuning of edge mode frequencies compared to the coupling of edge modes. The hybridization of edge modes is then obstructed and the smallest decay rate is comparable to γ , see Fig. 3c.

Even if we introduce moderate on-site disorder in the topological array ($\phi \neq 0, \pi$), we observe large hybridization of edge modes giving rise to long-lived elementary excitations for lasing at a frequency lying in the middle of the passive-system band gap (see Appendix D for more details). This is due to the robustness of edge modes and their frequencies against on-site disorder, whose level is smaller than the topological band gap [12, 16].

In general, long-lived elementary excitations appear due to the hybridization of edge modes for any topological model with a linear dispersion of edge-mode frequencies. The lifetime of elementary excitations can be suppressed by selecting a lasing frequency around which the dispersion of edge-mode frequencies is no longer linear. The long-lived elementary excitations will be shown in the next section to have crucial consequences for light coherence.

VII. COHERENCE PROPERTIES

We now discuss coherence properties of topological lasers and how they are influenced by long-lived elementary excitations, investigating the emission spectrum of pumped optical sites and the second-order autocorrelation function.

We start by studying the autocorrelation of complex optical amplitudes $\langle c_j(t) c_j^*(t + \Delta t) \rangle$. The dominant contribution in this autocorrelation is determined by phase fluctuations $\delta\theta_j$, where $c_j = (\bar{C}_j + \delta C) e^{i(-\Omega t + \bar{\theta}_j + \delta\theta_j)}$ and $\bar{c}_j = \bar{C}_j e^{i\bar{\theta}_j}$ (see Appendix C for more details). The amplitude fluctuations δC_j are negligible in comparison to the large mean-field occupation \bar{C}_j^2 [22]. Amplitude fluctuations δC_j and phase fluctuations $\delta\theta_j$ are linearly related to the fluctuations of complex amplitudes δc_j and δc_j^* as well as to the normal modes of elementary excitations

$$\begin{pmatrix} \delta C \\ \delta \Theta \end{pmatrix} = \mathcal{W} \mathcal{N}, \quad (8)$$

where $\delta\Theta_j = \bar{C}_j \delta\theta_j$, the vector \mathcal{N} contains the complex amplitudes of the normal modes and \mathcal{W} is the transformation matrix. This allows us to express the autocorrelations of complex optical amplitudes

$$\begin{aligned} \langle c_j(t) c_j^*(t + \Delta t) \rangle &\approx \bar{C}_j^2 e^{i\Omega\Delta t - |\Delta t|/\tau_c} \\ &+ \sum_{\alpha \neq \nu} n_\alpha |\mathcal{W}_{(j+N)\alpha}|^2 e^{i(\text{Re } \epsilon^{(\alpha)} + \Omega)\Delta t + \text{Im } \epsilon^{(\alpha)} |\Delta t|} \end{aligned} \quad (9)$$

in terms of the complex frequencies of elementary excitations $\epsilon^{(\alpha)}$ and the occupations $n_\alpha = \frac{1}{2|\text{Im } \epsilon^{(\alpha)}|} (\mathcal{R} \mathcal{R}^\dagger)_{\alpha\alpha}$ of the corresponding normal modes, where $\tau_c =$

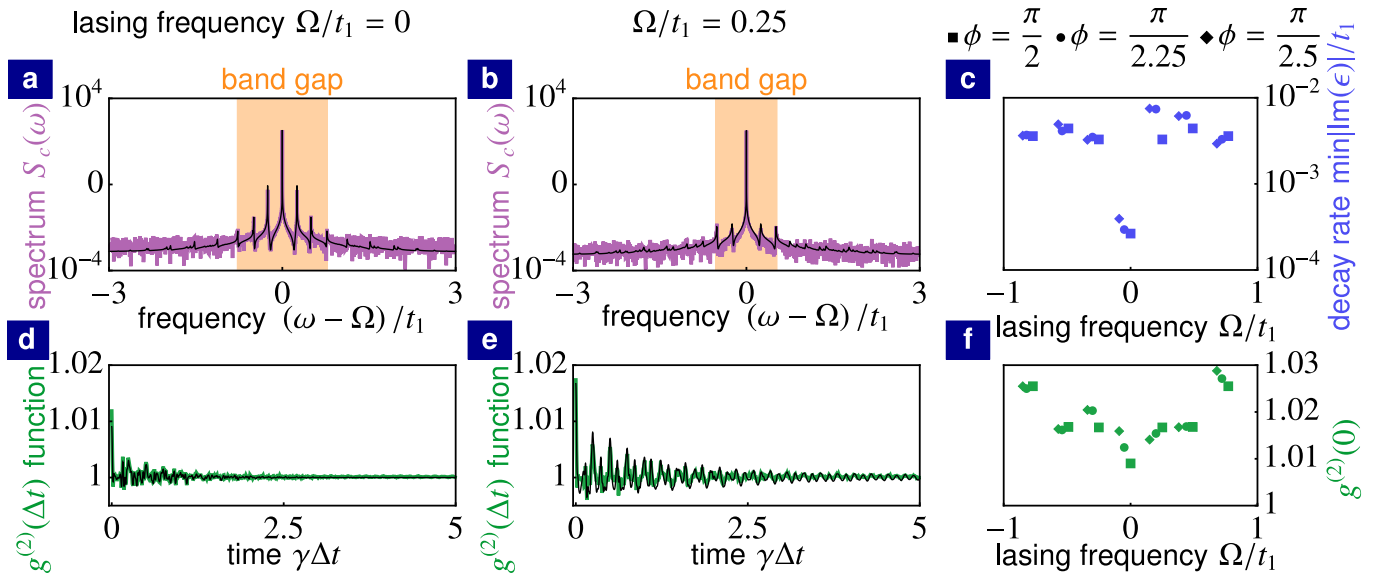


FIG. 3. Coherence properties of topological laser. (a) and (b) Optical spectrum of a pumped optical site lying at the edge of the topological array for lasing at the frequency $\Omega/t_1 = 0$ and at the frequency $\Omega/t_1 = 0.25$, respectively. Linearization of Langevin equations around the mean-field steady state (black line) and numerical simulations of nonlinear Langevin equations (purple line). The orange region shows the band gap in the spectrum of elementary excitations. (d) and (e) Second-order autocorrelation function of a pumped optical site lying at the edge of the topological array for lasing at the frequency $\Omega/t_1 = 0$ and at the frequency $\Omega/t_1 = 0.25$, respectively. Linearization of Langevin equations around the mean-field steady state (black line) and numerical simulations of nonlinear Langevin equations (green line). (c) Smallest decay rate of elementary excitations $\min_{\alpha \neq \nu} |\text{Im } \epsilon^{(\alpha)}|$ as a function of the lasing frequency Ω for Haldane flux $\phi = \pi/2$ (squares), $\phi = \pi/2.25$ (circles) and $\phi = \pi/2.5$ (diamonds). (f) Equal-time second-order autocorrelation function $g^{(2)}(0)$ as a function of the lasing frequency Ω for Haldane flux $\phi = \frac{\pi}{2}$ (squares), $\phi = \frac{\pi}{2.25}$ (circles) and $\phi = \frac{\pi}{2.5}$ (diamonds). (Parameters: $t_2/t_1 = 0.15$, $\gamma/t_1 = 0.01$, $g/t_1 = 0.05$, $I_{\text{sat}}\gamma/q = 25$; (a), (b), (d) and (e) $\phi = \pi/2$)

$2\bar{C}_j^2|\mathcal{W}_{(j+N)\nu}|^{-2}/(\mathcal{R}\mathcal{R}^\dagger)_{\nu\nu}$ is a coherence time, the index ν labels the non-decaying mode, and $\mathcal{R}\mathcal{R}^\dagger = \frac{1}{2}\mathcal{W}^{-1}\mathcal{Q}\mathcal{Q}^\dagger(\mathcal{W}^{-1})^\dagger$ is the correlation matrix for the normal modes (see Appendix C for a detailed derivation).

The optical spectrum $S_{c_j}(\omega)$ is the Fourier transform of the autocorrelation $\langle c_j(t)c_j^*(t+\Delta t) \rangle$. The light field emitted by optical sites is proportional to the complex amplitudes of the optical sites as described by input-output formalism [22]. As a result, the emission spectrum is proportional to the optical spectrum $S_{c_j}(\omega)$. The optical spectrum of a pumped optical site located at the edge of the array is shown in Figs. 3a and 3b for lasing at the frequency $\Omega/t_1 = 0$ and $\Omega/t_1 = 0.25$, respectively. We find a good quantitative agreement between the optical spectrum determined from the linearized Langevin equations (black lines), see Eq. (9), and the optical spectrum obtained from numerical simulations (purple line) of the nonlinear Langevin equations (1). The ensemble average $\langle c_j(t)c_j^*(t+\Delta t) \rangle$ can be replaced by a time average for a steady-state laser operation.

For lasing at both frequencies, the optical spectrum contains a central peak at the lasing frequency corresponding to the first term in Eq. (9). Undamped fluctuations in the phase of the lasing mode associated with the non-decaying normal mode of elementary excitations lead to a phase diffusion of light field, giving rise to a

Lorentzian shape of the central peak with a linewidth $2/\tau_c$ [22]. The linewidth is proportional to the strength of fluctuations q as well as inversely proportional to the number of pumped sites and the occupation of the pumped optical site \bar{C}_j^2 . The linewidth is approximately constant for lasing of any edge mode. Small deviations in the linewidth occur due to moderate discrepancies in the spatial profile $|\mathcal{W}_{ja}|^2$ of individual edge modes.

For lasing at the frequency $\Omega/t_1 = 0$ lying in the middle of the passive-system band gap, the optical spectrum contains also satellite peaks (see Fig. 3a). The satellite peaks appear due to the incoherent population of normal modes for elementary excitations, corresponding to the terms on the second line of Eq. (9). The occupation n_α of normal modes for elementary excitations is inversely proportional to the decay rate $|\text{Im } \epsilon^{(\alpha)}|$ and proportional to the strength of noise q . As a result, long-lived elementary excitations with a very small decay rate are largely populated giving rise to the satellite peaks in the optical spectrum. This large incoherent population of normal modes for elementary excitations leads to large phase fluctuations in the emitted light field decreasing its coherence.

Since elementary excitations are not dependent on the absolute scaling, I_{sat} , of the mean-field steady-state solution, the occupation of normal modes n_α does not depend

on the mean number of photons in the lasing mode \bar{n} . As a result, the height of the satellite peaks is also independent of the the mean number of photons in the lasing mode \bar{n} .

Our results show that large phase fluctuations and the decreased light coherence of emitted light field persist even when moderate on-site disorder is introduced (see Appendix D). This is due to the robustness of edge modes and their frequencies against disorder. As a result, long-lived elementary excitations with a very small decay rate and a large occupation n_α of the corresponding normal modes occur even if moderate on-site disorder is considered.

On the other hand, the incoherent population of elementary excitations and corresponding phase fluctuations can be suppressed by selecting a different lasing frequency. As it was shown in the previous section, the lifetime of elementary excitations is reduced by at least one order of magnitude for lasing at a frequency, which does not lie in the middle of the passive-system band gap, see Fig. 3c. As a result, the incoherent population of elementary excitations and the corresponding satellite peaks in the optical spectrum are suppressed (see Fig. 3b) leading to a larger coherence of emitted light than for $\Omega/t_1 = 0$.

The second-order autocorrelation function $g_j^{(2)}$ describes correlations in the intensity of emitted light at different times [22]. For a laser, it is desired that these intensity correlations vanish corresponding to $g_j^{(2)} = 1$. The second-order autocorrelation function is determined by amplitude fluctuations [22]

$$g_j^{(2)}(\Delta t) = \frac{\langle c_j(t)c_j(t + \Delta t)c_j^*(t + \Delta t)c_j^*(t) \rangle}{\langle c_j(t)c_j^*(t) \rangle \langle c_j(t + \Delta t)c_j^*(t + \Delta t) \rangle} = 1 + \frac{4}{\bar{C}_j^2} \langle \delta C_j(t) \delta C_j(t + \Delta t) \rangle + \mathcal{O}\left(\frac{1}{\bar{C}_j^4}\right). \quad (10)$$

Amplitude autocorrelations $\langle \delta C_j(t) \delta C_j(t + \Delta t) \rangle$ can be expressed in terms of normal modes' correlations (see Appendix C). The second-order autocorrelation function $g_j^{(2)}(\Delta t)$ for a pumped optical site located at the edge of the array is shown in Figs. 3d and 3e for lasing at the frequency $\Omega/t_1 = 0$ and $\Omega/t_1 = 0.25$, respectively. We compare the results determined from the linearized Langevin equations (black line) to numerical simulations (green line) of the nonlinear Langevin equations (1). The ensemble average $\langle c_j(t)c_j(t + \Delta t)c_j^*(t + \Delta t)c_j^*(t) \rangle$ can be replaced by a time average for a steady-state laser operation.

For lasing at both frequencies, the equal-time second-order autocorrelation function $g_j^{(2)}(0)$ is close to unity as expected for a laser, which is driven well above threshold. With the time difference Δt , $g_j^{(2)}(\Delta t)$ decays to unity at time comparable to $1/\gamma$. This shows that amplitude fluctuations correspond to fast-decaying elementary excitations. We can see that $g_j^{(2)}(0)$ and temporal oscil-

lations of $g_j^{(2)}(\Delta t)$ are larger for lasing at the frequency $\Omega/t_1 = 0.25$ than for lasing at the frequency $\Omega/t_1 = 0$ lying in the middle of the band gap.

In Fig. 3f, we plot $g_j^{(2)}(0)$ as a function of the lasing frequency Ω for different values of the Haldane flux. One can see that $g_j^{(2)}(0)$ is, in general, moderately larger for lasing at a frequency which does not lie in the middle of the band gap for all values of the Haldane flux. This shows that lasing at these frequencies leads to moderately larger amplitude fluctuations.

VIII. EXPERIMENTAL PARAMETERS

We estimate parameters of our model (1) to be relevant for recent experiments [9]. Typical parameters for arrays of coupled microring resonators are the decay rate $\gamma \sim 1$ GHz and the hopping amplitude $t_1 \sim 100$ GHz with a feasible ratio $\gamma/t_1 \sim 0.01$ [16]. For two-dimensional topological arrays with the total number of microring resonators $N \sim 100$ (as implemented in Ref. [9]), the frequency separation of edge modes is typically larger than their linewidth.

The dominant source of noise in pumped optical sites is the spontaneous emission at rate $q \sim 100$ GHz [23]. A typical circulating power in the lasing mode of a single microring resonator is $P_c \sim 1$ mW which corresponds to a typical number of photons $\bar{n} \sim 10^3$ in the lasing mode [23]. We conclude that our model with $I_{\text{sat}}\gamma/q \sim 10$ describes an experimentally-relevant relative strength of noise compared to the number of photons in the lasing mode.

IX. CONCLUSIONS

We have demonstrated that long-lived elementary excitations, which emerge due to the hybridization of topological edge modes, lead to large phase fluctuations and a decrease in the coherence of the emitted light field. Even though we focus in our manuscript on the Haldane model, long-lived elementary excitations appear for any topological model if the dispersion of edge-mode frequencies is approximately linear around the lasing frequency. Since topological edge modes and their frequencies are robust against disorder, the long-lived elementary excitations appear even in the presence of moderate on-site disorder. Our results for the Haldane model show that the deviation from a linear dispersion around lasing frequencies, which do not lie in the middle of the passive-system band gap, is sufficient to obstruct the hybridization of edge modes. As a result, the lifetime of elementary excitations is reduced by orders of magnitude and the phase fluctuations are largely suppressed. On the other hand, this leads to a moderate increase of amplitude fluctuations and the second-order autocorrelation function. However, the second-order autocorrelation function still

remains close to unity. In the future, different topological models can be studied to provide insight into how elementary excitations in topological lasers are affected by the presence of several topological band gaps supporting edge modes with opposite chirality [1], a pseudospin degree of freedom in pseudo quantum spin Hall systems [16, 24] or topological lasing in synthetic dimensions [3].

APPENDIX A: NON-DECAYING MODE

Here we discuss the hybridization of two passive-system normal modes which are formed from the lasing mode, giving rise to the non-decaying mode. We label the lasing mode by the index l . Since $\omega_l = \Omega$, the pair of passive-system normal modes is degenerate $\epsilon_p^{(l)} = \tilde{\epsilon}_p^{(l)} = 0$ leading to a large hybridization of the pair. The lasing mode coincides with the mean-field steady-state solution $e_j^{(l)} \approx \bar{c}_j e^{i\varphi} / \sqrt{\bar{n}}$, where \bar{n} is the mean number of photons in the lasing mode and φ is an arbitrary phase. This gives

$$\bar{\Gamma}_{ll} = \tilde{\Delta}_{ll} e^{2i\varphi} = g \sum_{j=1}^N \mathbb{P}_j \frac{|\bar{c}_j|^4}{\left(1 + \frac{|\bar{c}_j|^2}{\bar{I}_{\text{sat}}}\right)^2}, \quad (\text{A1})$$

and $\delta\Gamma_{ll}$ trivially vanishes. Using also $\bar{\omega}_{ll} = 0$ and $\delta\omega_{ll} = 0$, we see from Eq. (7) that the hybridization of this mode pair gives rise a non-decaying mode with the complex frequency $\epsilon_+^{(l,l)} = 0$ and a fast-decaying mode with the complex frequency $\epsilon_-^{(l,l)} = -2i\bar{\Gamma}_{ll}$.

APPENDIX B: HALDANE FLUX $\phi = \pi/2$

The value of the Haldane flux $\phi = \pi/2$ represents a special case because the Hamiltonian \mathbf{H} of the passive system then exhibits the following symmetry $\mathbf{S} \mathbf{H} \mathbf{S} = -\mathbf{H}^*$, where \mathbf{S} is a unitary matrix and $\mathbf{S}^2 = \mathbb{1}$. The unitary transformation \mathbf{S} introduces the phase shift π between the two sublattices of the Haldane model, i.e. $c_j \rightarrow c_j$ for sublattice A and $c_j \rightarrow -c_j$ for sublattice B . Due to this symmetry, the spectrum of the passive system consists of a zero frequency and frequency pairs $(\omega_m, \omega_{\tilde{m}})$, $\omega_{\tilde{m}} = -\omega_m$. As a result, all passive-system normal modes are pairwise degenerate for $\Omega/t_1 = 0$ leading to the hybridization of all degenerate pairs described by the 2×2 dynamical matrix $\mathcal{D}^{(m, \tilde{m})}$, see Eq. (6). As the unitary \mathbf{S} introduces only a local phase shift, $|e_j^{(m)}| = |e_j^{(\tilde{m})}|$ leading to $\bar{\Gamma}_{m\tilde{m}} = \tilde{\Gamma}_{mm} = \tilde{\Gamma}_{\tilde{m}\tilde{m}}$ and $\delta\Gamma_{m\tilde{m}} = 0$. Using also $\delta\omega_{m\tilde{m}} = 0$, the complex frequencies of hybridized modes are $\epsilon_{\pm}^{(m, \tilde{m})} = \omega_m + i(\bar{\Gamma}_{mm} \pm |\tilde{\Delta}_{m\tilde{m}}|)$. Since the coupling $\tilde{\Delta}_{mn}$ between bulk modes is small, the hybridization leads to a small splitting in imaginary parts of complex frequencies for bulk modes (grey lines in Fig. 2c). On the other hand, the large coupling of edge modes leads to a large splitting in the imaginary parts of complex frequencies (blue lines in Fig. 2c).

APPENDIX C: CORRELATIONS OF AMPLITUDE AND PHASE FLUCTUATIONS

Here, we provide details about how the optical spectrum and the second-order autocorrelation function are derived and how they are related to the normal modes of elementary excitations.

It is convenient to study noise in terms of amplitude and phase fluctuations, due to the $U(1)$ symmetry of the mean-field dynamical equations, $c_j \rightarrow c_j e^{i\varphi}$, where φ is an arbitrary overall phase. The coherence properties of a laser driven well above threshold are directly determined by the correlations in amplitude fluctuations and phase fluctuations [22]. Amplitude fluctuations δC_j and phase fluctuations $\delta\theta_j$ are linearly related to the fluctuations of complex amplitudes δc_j and δc_j^*

$$\delta C_j = \frac{e^{-i\bar{\theta}_j} \delta c_j + e^{i\bar{\theta}_j} \delta c_j^*}{2}, \quad \delta\theta_j = \frac{e^{-i\bar{\theta}_j} \delta c_j - e^{i\bar{\theta}_j} \delta c_j^*}{2i\bar{C}_j}, \quad (\text{C1})$$

where $\bar{c}_j = \bar{C}_j e^{i\bar{\theta}_j}$. This relation can be described by the linear transformation

$$\begin{pmatrix} \delta \mathbf{C} \\ \delta \boldsymbol{\Theta} \end{pmatrix} = \mathcal{T} \begin{pmatrix} \delta \mathbf{c} \\ \delta \mathbf{c}^* \end{pmatrix}, \quad (\text{C2})$$

where $\delta\Theta_j = \bar{C}_j \delta\theta_j$. The linearized Langevin equations around the mean-field steady-state for the amplitude and phase fluctuations are

$$i \frac{d}{dt} \begin{pmatrix} \delta \mathbf{C} \\ \delta \boldsymbol{\Theta} \end{pmatrix} = \mathcal{T} \mathcal{D} \mathcal{T}^{-1} \begin{pmatrix} \delta \mathbf{C} \\ \delta \boldsymbol{\Theta} \end{pmatrix} + \frac{i}{\sqrt{2}} \mathcal{Q} \begin{pmatrix} \mathbf{C}_{\text{in}} \\ \boldsymbol{\Theta}_{\text{in}} \end{pmatrix}, \quad (\text{C3})$$

where \mathbf{C}_{in} and $\boldsymbol{\Theta}_{\text{in}}$ describe real-valued Gaussian white noise, with following correlations $\langle C_{j,\text{in}}(t) C_{k,\text{in}}(t') \rangle = \delta_{jk} \delta(t - t')$, $\langle \Theta_{j,\text{in}}(t) \Theta_{k,\text{in}}(t') \rangle = \delta_{jk} \delta(t - t')$, and $\langle C_{j,\text{in}}(t) \Theta_{k,\text{in}}(t') \rangle = 0$. Amplitude and phase fluctuations are linearly related to the normal modes of elementary excitations

$$\begin{pmatrix} \delta \mathbf{C} \\ \delta \boldsymbol{\Theta} \end{pmatrix} = \mathcal{W} \mathcal{N}, \quad (\text{C4})$$

where $\mathcal{W} = \mathcal{V} \mathcal{T}$, columns of the matrix \mathcal{V} are the normal modes of elementary excitations $\mathcal{E}^{(\alpha)}$ described in Sec. IV and the vector \mathcal{N} contains the complex amplitudes of these normal modes. Non-equal-time phase and amplitude autocorrelations can be expressed in terms of normal modes' correlations

$$\langle \delta C_j(t) \delta C_j(t + \Delta t) \rangle = \sum_{\alpha, \beta=1}^{2N} \mathcal{W}_{j\alpha} \langle \mathcal{N}_\alpha(t) \mathcal{N}_\beta^*(t + \Delta t) \rangle \mathcal{W}_{\beta j}^\dagger, \quad (\text{C5})$$

$$\begin{aligned} & \langle [\delta\theta_j(t) - \delta\theta_j(t + \Delta t)]^2 \rangle \\ &= \frac{1}{\bar{C}_j^2} \sum_{\alpha, \beta=1}^{2N} \mathcal{W}_{(j+N)\alpha} \langle |\mathcal{N}_\alpha(t) - \mathcal{N}_\beta(t + \Delta t)|^2 \rangle \mathcal{W}_{\beta(j+N)}^\dagger. \end{aligned} \quad (\text{C6})$$

The correlations of normal modes are

$$\langle \mathcal{N}_\alpha(t) \mathcal{N}_\beta^*(t + \Delta t) \rangle = \frac{i (\mathcal{R} \mathcal{R}^\dagger)_{\alpha\beta}}{(\epsilon^{(\beta)})^* - \epsilon^{(\alpha)}} e^{i\epsilon^{(\alpha)} \Delta t}, \quad \Delta t < 0, \quad (\text{C7})$$

$$\langle \mathcal{N}_\alpha(t) \mathcal{N}_\beta^*(t + \Delta t) \rangle = \frac{i (\mathcal{R} \mathcal{R}^\dagger)_{\alpha\beta}}{(\epsilon^{(\beta)})^* - \epsilon^{(\alpha)}} e^{i(\epsilon^{(\beta)})^* \Delta t}, \quad \Delta t > 0, \quad (\text{C8})$$

for all normal modes α and β except from the autocorrelation of the non-decaying mode, i.e. for $\alpha = \beta = \nu$ and $\epsilon^{(\nu)} = 0$. Note that the non-decaying mode is related only to phase fluctuations. As a result, the relevant autocorrelation of the non-decaying mode is

$$\langle |\mathcal{N}_\nu(t) - \mathcal{N}_\nu(t + \Delta t)|^2 \rangle = (\mathcal{R} \mathcal{R}^\dagger)_{\nu\nu} |\Delta t|. \quad (\text{C9})$$

The dominant contribution in the autocorrelation of complex optical amplitudes reads

$$\langle c_j(t) c_j^*(t + \Delta t) \rangle \approx \bar{C}_j^2 e^{i\Omega\Delta t} e^{-\langle [\delta\theta_j(t) - \delta\theta_j(t + \Delta t)]^2 \rangle / 2}, \quad (\text{C10})$$

where amplitude fluctuations are neglected, since they are small in comparison to the large mean-field occupation \bar{C}_j^2 [22]. Using Eq. (C6), we express $\langle [\delta\theta_j(t) - \delta\theta_j(t + \Delta t)]^2 \rangle$ in terms of correlations in the normal modes of elementary excitations (C7), (C8) and (C9) to derive the optical spectrum Eq. (9) in the main text, where we neglect correlations between different normal modes $\langle |\mathcal{N}_\alpha(t) - \mathcal{N}_\beta(t + \Delta t)|^2 \rangle$ for $\alpha \neq \beta$. Only long-lived elementary excitations have significant contribution to the optical spectrum due to their large occupation n_α . Since the corresponding normal modes are formed from edge modes, they have a large detuning in the real parts of complex frequencies, which suppresses the correlations between different normal modes $\langle |\mathcal{N}_\alpha(t) - \mathcal{N}_\beta(t + \Delta t)|^2 \rangle$ for $\alpha \neq \beta$.

Similarly, we can express the second-order autocorrelation function (10) in terms of correlations in the normal modes of elementary excitations.

APPENDIX D: DISORDER

Here we study effects of moderate on-site disorder on the spectrum of elementary excitations and long-lived elementary excitations. We consider lasing at a frequency, which lies in the middle of the passive-system band gap. On-site disorder is represented by a Gaussian distribution of on-site frequencies ω_j with a zero mean value and a standard deviation σ . We consider moderate disorder with the standard deviation σ smaller than the size of the passive-system band gap $6\sqrt{3}t_2 \sin \phi$ but larger than the decay rate γ and gain g .

We compare the spectrum of elementary excitations for 30 disorder realizations and the spectrum of elementary excitations without disorder in Fig. D4a. The large

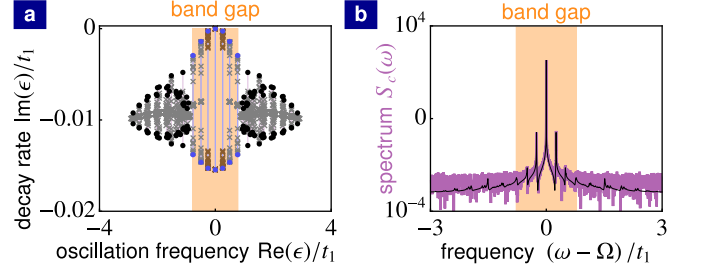


FIG. D4. Effects of moderate disorder. (a) Complex spectrum of elementary excitations for 30 disorder realizations (brown and gray crosses) for $\Omega/t_1 \approx 0$ compared to complex spectrum of elementary excitations without disorder with band gap (orange region), bulk modes (black points) as well as edge modes (blue points) for the lasing frequency $\Omega/t_1 = 0$. Purple and blue lines show the splitting in imaginary parts of complex frequencies due to the hybridization of bulk modes and edge modes, respectively. (b) Optical spectrum of a pumped optical site lying at the edge of the topological array for a single disorder realization and for lasing at the frequency $\Omega/t_1 = 0.01$. Linearization of Langevin equations around the mean-field steady state (black line) and numerical simulations of non-linear Langevin equations (purple line). The orange region shows the band gap in the spectrum of elementary excitations. (Parameters: (a) and (b) $t_2/t_1 = 0.15$, $\phi = \pi/2$, $\gamma/t_1 = 0.01$, $g/t_1 = 0.05$, $\sigma/t_1 = 0.1$; (b) $I_{\text{sat}}\gamma/q = 25$, $\Omega = 0.01$)

hybridization of edge modes with frequencies close to the lasing frequency leads to long-lived elementary excitations with a very small decay rate for all disorder realizations (brown crosses). This shows the robustness of long-lived elementary excitations against disorder. The incoherent occupation n_α of the corresponding slowly-decaying normal modes is large even in the presence of moderate on-site disorder and it leads to satellite peaks in the optical spectrum, see Fig. D4b.

ACKNOWLEDGMENT

We thank D. Malz for insightful discussions. This work was supported by the European Union's Horizon 2020 research and innovation programme under grant agreement No 732894 (FET Proactive HOT). A.N. holds a University Research Fellowship from the Royal Society and acknowledges support from the Winton Programme for the Physics of Sustainability.

NOTE ADDED

During the final stage of this project, a preprint [25] appeared, investigating coherence properties of topological lasers. Their numerical analysis of topological lasing in arrays of large sizes complements our study of topological lasing reported here.

[1] T. Ozawa, H. M. Price, A. Amo, N. Goldman, M. Hafezi, L. Lu, M. C. Rechtsman, D. Schuster, J. Simon, O. Zilbermanberg, and I. Carusotto, *Rev. Mod. Phys.* **91**, 015006 (2019).

[2] V. M. Martinez Alvarez, J. E. Barrios Vargas, M. Berdakin, and L. E. F. Foa Torres, *Eur. Phys. J. Spec. Top.* **227**, 1295 (2018).

[3] E. Lustig, S. Weimann, Y. Plotnik, Y. Lumer, M. A. Bandres, A. Szameit, and M. Segev, *Nature* **567**, 356 (2019).

[4] D. Smirnova, D. Leykam, Y. Chong, and Y. Kivshar, *arXiv:1912.01784* (2019).

[5] P. St-Jean, V. Goblot, E. Galopin, A. Lemaître, T. Ozawa, L. L. Gratiet, I. Sagnes, J. Bloch, and A. Amo, *Nat. Photonics* **11**, 651 (2017).

[6] M. Parto, S. Wittek, H. Hodaei, G. Harari, M. A. Bandres, J. Ren, M. C. Rechtsman, M. Segev, D. N. Christodoulides, and M. Khajavikhan, *Phys. Rev. Lett.* **120**, 113901 (2018).

[7] H. Zhao, P. Miao, M. H. Teimourpour, S. Malzard, R. El-Ganainy, H. Schomerus, and L. Feng, *Nat. Commun.* **9**, 981 (2018).

[8] B. Bahari, A. Ndao, F. Vallini, A. E. Amili, Y. Fainman, and B. Kanté, *Science* **358**, 636 (2017).

[9] M. A. Bandres, S. Wittek, G. Harari, M. Parto, J. Ren, M. Segev, D. N. Christodoulides, and M. Khajavikhan, *Science* **359**, eaar4005 (2018).

[10] S. Klembt, T. H. Harder, O. A. Egorov, K. Winkler, R. Ge, M. A. Bandres, M. Emmerling, L. Worschech, T. C. H. Liew, M. Segev, C. Schneider, and S. Höfling, *Nature* **562**, 552 (2018).

[11] Y. Zeng, U. Chattopadhyay, B. Zhu, B. Qiang, J. Li, Y. Jin, L. Li, A. G. Davies, E. H. Linfield, B. Zhang, Y. Chong, and Q. J. Wang, *Nature* **578**, 246 (2020).

[12] G. Harari, M. A. Bandres, Y. Lumer, M. C. Rechtsman, Y. D. Chong, M. Khajavikhan, D. N. Christodoulides, and M. Segev, *Science* **359**, eaar4003 (2018).

[13] S. Longhi, Y. Kominis, and V. Kovanis, *EPL* **122**, 14004 (2018).

[14] M. Secli, M. Capone, and I. Carusotto, *Phys. Rev. Research* **1**, 033148 (2019).

[15] H. Haken, *Light (Volume 2)* (North-Holland Physics Publishing, Amsterdam, 1985).

[16] M. Hafezi, S. Mittal, J. Fan, A. Migdall, and J. M. Taylor, *Nat. Photonics* **7**, 1001 (2013).

[17] F. D. M. Haldane, *Phys. Rev. Lett.* **61**, 2015 (1988).

[18] G. Jotzu, M. Messer, R. Desbuquois, M. Lebrat, T. Uehlinger, D. Greif, and T. Esslinger, *Nature* **515**, 237 (2014).

[19] P. G. Savvidis, C. Ciuti, J. J. Baumberg, D. M. Whittaker, M. S. Skolnick, and J. S. Roberts, *Phys. Rev. B* **64**, 075311 (2001).

[20] N. R. Bernier, E. G. Dalla Torre, and E. Demler, *Phys. Rev. Lett.* **113**, 065303 (2014).

[21] N. R. Bernier, L. D. Tóth, A. K. Feofanov, and T. J. Kippenberg, *Phys. Rev. A* **98**, 023841 (2018).

[22] C. W. Gardiner and P. Zoller, *Quantum Noise*, Springer Series in Synergetics (Springer, Berlin/Heidelberg, 2004).

[23] H. Hodaei, M.-A. Miri, M. Heinrich, D. N. Christodoulides, and M. Khajavikhan, *Science* **346**, 975 (2014).

[24] M. Hafezi, E. A. Demler, M. D. Lukin, and J. M. Taylor, *Nat. Phys.* **7**, 907 (2011).

[25] I. Amelio and I. Carusotto, *arXiv:1911.10437* (2019).